Realization of a tunable fiber-based double cavity system

T. Herzog,[1] S. Böhrkircher,[2] S. Both,[2] M. Fischer,[1] R. Sittig,[1] M. Jetter,[1] S. L. Portalupi,[1] T. Weiss,[2] and P. Michler[1]
[1]*Institut für Halbleiteroptik und Funktionelle Grenzflächen (IHFG), Center for Integrated Quantum Science and Technology (IQ^{ST}), and SCoPE, University of Stuttgart, Allmandring 3, 70569 Stuttgart, Germany*
[2]*4th Physics Institute and SCoPE, University of Stuttgart, Pfaffenwaldring 57, 70569 Stuttgart, Germany*

(Received 20 October 2020; accepted 15 December 2020; published 30 December 2020)

Tunable cavities have proven to be highly attractive systems in cavity quantum electrodynamics thanks to their performance and flexibility. The possibility to form a cavity around any emitter while simultaneously spectrally matching the chosen transitions makes these cavities an important tool in photonic quantum technology. In this paper, we report on the experimental realization and theoretical description of a fiber-based resonator with two spatially and spectrally distinct cavity modes. The careful design of the structures was performed via finite-element simulations. Thanks to the intrinsic tunability of the system, one mode can be brought in resonance with the second one, forming a supermode resulting in a hybridized two-mode pattern in the emission spectrum. For its realization, we combine a monolithic bottom cavity, formed by two distributed Bragg reflectors, with a top movable fiber mirror forming an externally tunable cavity mode. When tuning the top cavity in resonance with the monolithic bottom one, the cavity modes exhibit a pronounced anticrossing behavior typical for mode hybridization. Differently from a standard open cavity, when embedding single emitters—in this case, InGaAs quantum dots—in the structure, the Purcell factor is not uniform for each wavelength. Furthermore, we find a strong influence of the simulated Purcell factor, as well as of the measured light extraction, depending on the placement of the emitter in the top or in the bottom cavity. The discussed two-mode cavity could be employed for simultaneously Purcell-enhancing multiple transitions of an emitter while preserving the single-photon nature of the emitters inside the device.

DOI: 10.1103/PhysRevB.102.235306

I. INTRODUCTION

Optical microcavities [1] have proven their usefulness in quantum optics and cavity quantum electrodynamics, both by enhancing the performance of single emitters via the Purcell effect [2] or by entering the strong-coupling regime [3]. Various geometries are investigated and utilized, among which micropillar structures [4–8], photonic crystal cavities [9], and microspheres [10] are the most prominent ones. Thanks to highly developed semiconductor fabrication capabilities, these optical resonators reached top performances with high fabrication yield. Their monolithic nature provides stability but requires a careful design when employed with single emitters in order to ensure spatial and spectral matching between the cavity resonances and the emitter. This can be ensured utilizing deterministic fabrication techniques [11–14]. Still, the overall number of devices is orders of magnitude lower with respect to the available emitters in the utilized chip.

While in these monolithic cavities the modes are fixed by the geometrical design, the advantage of open cavities lies in their intrinsic tunability, which allows adapting the cavity dimensions to the embedded emitter. Open cavities have been employed together with various emitters including nitrogen vacancy centers [15,16], quantum wells [17], and quantum dots (QDs). In the latter case the predominant approach is utilizing an open cavity via a silica template [18,19], coupling the emission afterwards into an optical fiber. In this way, even the strong-coupling regime could be exploited [20]. A different approach, like the one employed in this paper, is based on the fabrication of an external mirror directly on a fiber end facet, thus forming a fiber-based open cavity [21] with embedded QDs as emitters [22–24]. These types of tunable cavities have been shown to be a valid approach to explore cavity quantum electrodynamics (cQED) reaching performances comparable to those of their monolithic counterparts.

Typically, the fundamental mode of the cavity is exploited in the experiments while the higher-order modes are so far away in frequency that they do not interact with the two-level system. This means that when more transitions from the same emitter need to be manipulated via cQED, it is not simply possible to design a cavity that employs the fundamental and the first-order modes, since their splitting is typically much larger than the wavelength mismatch between different emitter transitions, typically 2–3 nm for an exciton and biexciton in a QD. A few approaches utilized coupled cavities to create a doublet of hybridized modes (for example, coupled micropillars [25], microdisks [26,27], and photonic crystals [28]): The two modes of the respective cavities when brought together lead to the formation of coupled modes. This approach requires a fabrication processing that is even more complex than for a single-mode cavity, in order to ensure the simultaneous frequency matching of both modes with multiple transitions of an emitter.

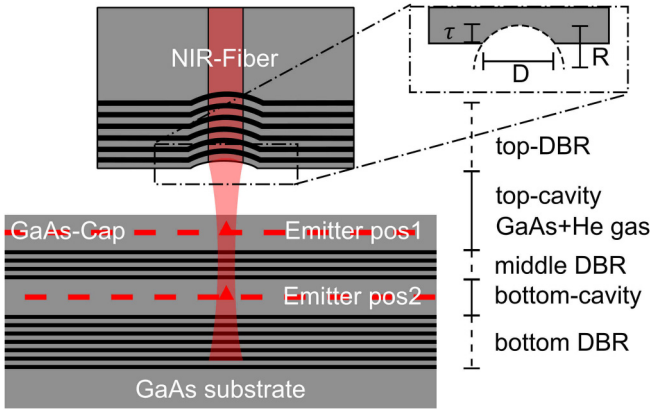

FIG. 1. Schematic picture of the investigated double cavity structures. The device is based on two coupled cavities: one monolithic part—the bottom cavity—formed by two distributed Bragg reflectors (bottom and middle DBRs) with a GaAs cap spacer, and an open cavity—the top cavity—utilizing the middle DBR of the monolithic sample as well as a high-reflection coated end facet of an optical fiber as the top mirror. In the proper configuration a supermode can manifest between both cavities leading to hybridization of the two cavity modes. Two cases are here investigated, namely, when the quantum dot emitters are placed in the bottom [emitter position (pos) 2] or in the top (emitter position 1) cavity, respectively. In both configurations, the emitters, in this case quantum dots, are optimally placed in the electric-field maximum of the respective cavity.

An alternative strategy relies on the use of a stacked Fabry-Perot double cavity [29–32] as has been demonstrated utilizing quantum wells as the active medium [33]. In this paper, we push this approach even further by replacing the top cavity with an external tunable fiber mirror and employing QDs as single-photon emitters. We will show the possibility to actively tune the modes into resonance, showing the expected hybridization and furthermore combining the aforementioned advantage of having a tunable open-cavity structure to gain more insight into the mode behavior.

II. DEVICE STRUCTURE

The double cavity structure consists of a monolithic part, i.e., the sample, as well as an open tunable part, namely, the end facet of an optical fiber coated to be highly reflective. The sample is grown via metal-organic vapor phase epitaxy. In detail (see Fig. 1), on top of a GaAs wafer, the bottom distributed Bragg reflector (DBR), consisting of alternating layer pairs of AlAs/GaAs, is deposited. The bottom cavity is formed by adding a GaAs spacer and a second DBR structure. The second DBR will constitute the middle mirror in the two-cavity experiments. The dimension of this cavity is designed to be resonant with the wavelength of a possible emitter in its active region in the absence of the top cavity. The sample is finished by a capping layer of GaAs. The investigated geometries include In(Ga)As QDs at two different positions: either in the bottom cavity (i.e., emitter position 2 in Fig. 1, placed between the bottom and middle DBRs) or in the top cavity (i.e., emitter position 1, the cavity formed by the middle DBR and the external fiber-based mirror). The emitters are placed in such a way that the electric-field maximum of the respective cavity coincides with the emitter position to ensure a good emitter-cavity coupling. The top mirror of the double cavity consists of a coated end facet of a standard near-infrared (NIR) fiber. Focused-ion-beam milling [34] is used to create a curved surface where alternating layers of Ta_2O_5/SiO_2 are then deposited. For an easier angular alignment, the fiber is prestructured with a parabolic imprint which can be approximated by a sphere as shown in Fig. 1. The position of the top fiber with respect to the sample can be precisely controlled, allowing formation of a cavity around each emitter on the sample, while further adjusting the cavity distance to ensure spectral resonance between the cavity mode and the emitter's transitions. High positioning accuracy and mechanical stability are achieved by placing the sample on xy, z piezoelectric positioners (attocube systems AG) with a subnanometric resolution as described in detail in a previous work [24]. In order to ensure emission towards the fiber and to have good coupling conditions between the resonators, the reflectivities of the mirrors are selected as

$$\mathrm{DBR}_{\mathrm{middle}} \ll \mathrm{DBR}_{\mathrm{top}} < \mathrm{DBR}_{\mathrm{bottom}}. \tag{1}$$

III. SIMULATIONS

For our simulations, we use a finite-element solver [35] to model the double cavity and determine the modes inside the system. The double cavity is simulated with a diameter $D = 9\ \mu$m, a curved fiber mirror with ten double layers of Ta_2O_5/SiO_2 and an imprint depth of $\tau = 0.7\ \mu$m, a radius of curvature $R = 14.5\ \mu$m, a vacuum or He exchange gas layer of thickness between 6 and 8 μm as the top cavity, a 261-nm-thick GaAs capping layer on top of the middle DBR, nine layers of GaAs/AlAs for the middle DBR, a 242-nm-thick GaAs layer for the bottom cavity, and 32 GaAs/AlAs pairs for the bottom mirror (see Fig. 1). We use refractive indices of $n_{\mathrm{GaAs}} = 3.498$ [36] and $n_{\mathrm{AlAs}} = 2.935$ [36] (both adapted to 4 K), $n_{\mathrm{Ta_2O_5}} = 2.086$ [37], and $n_{\mathrm{SiO_2}} = 1.452$ [38] for the different materials. By exploiting the rotational symmetry of the system and using cylindrical coordinates (r, ϕ, z), the calculation domain can be reduced to the r-z plane. The cavity is embedded in a shell of perfectly matched layers to account for the openness of the system, i.e., the coupling to the environment. We obtain the modes by performing an eigenmode analysis of the cavity system. Afterwards, we can calculate the quality factor of the modes through their complex resonance frequency ν,

$$Q = -\frac{\mathrm{Re}(\nu)}{2\,\mathrm{Im}(\nu)}. \tag{2}$$

To determine how much signal couples into the fiber (τ_{in}), we calculate the overlap between the electric fields in the cavity and the eigenmode of the optical fiber. The result is normalized to the intensity exiting the cavity to the top.

The Purcell enhancement F_p can be calculated by

$$F_p = \frac{3c^3\mathrm{Re}(Q)}{4\pi^2 n^3 \nu^3 \mathrm{Re}(V)}, \tag{3}$$

with c being the speed of light, n being the refractive index of the reference material (for the simulations we took vacuum), and V being the mode volume of the resonant mode, which depends on the position and orientation of the quantum

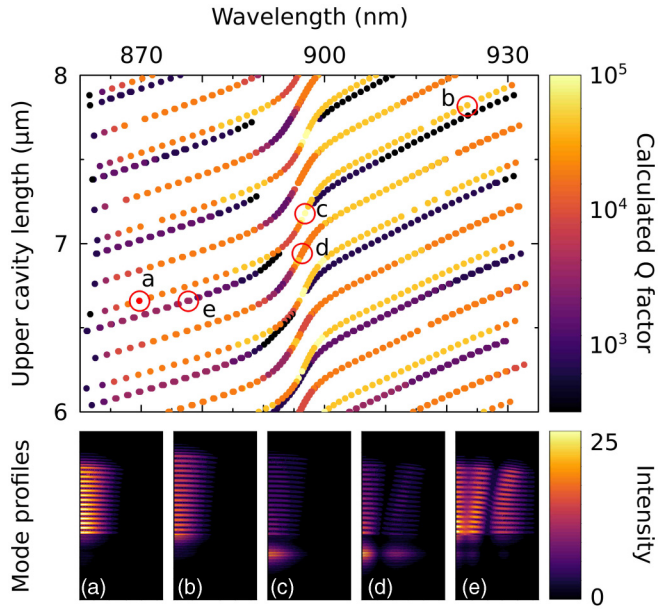

FIG. 2. Calculated quality factors of the double cavity structure for various different cavity lengths of the upper cavity. In the anticrossing region the Q factor is highly sensitive to the wavelength. Maximum Q factors of 100 000 can be achieved. Each depicted data point corresponds to a mode-field simulation. Exemplary mode profiles: For (a) and (b), light is mainly confined in the upper cavity; in (c) and (d), light is confined in the upper and lower cavities forming a supermode; and (d) and (e) depict higher-order transverse modes. Quality factors corresponding to (a)–(e) can be found in Table I.

emitter. The mode volume V was calculated following Sauvan *et al.* [39] as an integral of the fields over the whole structure including perfectly matched layers,

$$V = \frac{\int \mathbf{E} \cdot \mathbf{D}}{\varepsilon_0 n^2 [\mathbf{E}(\mathbf{r}_0)\mathbf{e}_r]^2} dV. \tag{4}$$

We assume nondispersive materials. The quantum emitter is placed at position $\mathbf{r}_0$ and oriented in the radial direction with unit vector $\mathbf{e}_r$. Calculated Q factors for different cavity lengths and wavelengths are displayed in Fig. 2. The Q factors for the modes shown in Figs. 2(a)–2(e) as well as the corresponding incoupling efficiencies and Purcell factors are listed in Table I. With the help of field plots [Figs. 2(a)–2(e)], we can discern longitudinal modes [Figs. 2(a) and 2(b)] as well as higher-order transverse modes, i.e., Laguerre-Gauss modes with radial index $p = 1$ as shown in Fig. 2(d) and $p = 2$ as shown in Fig. 2(e). Modes with azimuthal index $l \neq 0$ are not considered since they do not couple to the emitter. Coupling and anticrossing occur only between modes with the same symmetries, not between the longitudinal and higher-order transverse modes. While also for transverse modes an anticrossing behavior can be observed, the main interest is put on the longitudinal modes due to their possible applications. The modes mainly manifest in the upper cavity, while in the anticrossing region, where both cavities are in resonance [Fig. 2(c)], a supermode between both cavities is formed.

The mode splitting strongly depends on the coupling strength. If the splitting is too high, the modal separation is large, too. Therefore the mirrors must be designed to yield a coupling strength that is at a critically low level, which is yet high enough to be above the weak-coupling regime between the top and bottom cavities. The modal splitting then can be designed by fine-tuning this coupling strength.

TABLE I. Quality factor Q, calculated incoupling efficiency τ_{in}, and Purcell factor F in the top and bottom cavities for selected positions in Figs. 2 and 3. In addition to longitudinal (long.) modes, transverse modes are listed. Here, p corresponds to the radial index of the Laguerre-Gauss mode. The positions with asterisks correspond to Q factors found via the experimental results. The errors stem from the low brightness and therefore a bad signal-to-noise ratio.

Simulation results					
Position	Mode type	Q	τ_{in}	F_{bottom}	F_{top}
a	long.	21000	0.272	0.465	5.231
b	long.	44047	0.258	5.779	66.457
c	long.	91564	0.202	94.000	5.686
d	$p = 1$	22651	0.083	14.898	0.088
e	$p = 2$	4072	0.014	0.165	0.629

Experimental results		
Position	Mode type	Q
a*	long.	4324 ± 31
c*	long.	9771 ± 1928
f*	long.	6252 ± 84
g*	long.	7506 ± 188

IV. EXPERIMENTAL RESULTS

Following the simulation results of the previous paragraph, two double cavity systems with the aforementioned parameters were fabricated. Simulation and experimental results are shown in Fig. 3. In one case [Figs. 3(a) and 3(b)] the emitters feeding the cavity are placed in the top cavity, while in the second case [Figs. 3(c) and 3(d)], the emitters are placed in the bottom cavity. Comparing the simulation results [Figs. 3(a) and 3(c)] for these two cases, it is evident that the mode propagation (x and y coordinates of the data points in the plot) is identical for both cases since the cavity geometry and dimensions are the same. Exemplary quality factors and expected Purcell enhancement as well as incoupling efficiencies for selected points are displayed in Table I. Interestingly, the calculated intensity (color-coded z component)—given by the Purcell enhancement times the coupling efficiency to the fiber—is fundamentally different. Whereas in the case where the QDs are located in the upper cavity, the Purcell enhancement in the anticrossing regime is suppressed, conversely, we find significant Purcell enhancement in the anticrossing region when the emitters are placed in the bottom cavity. This can be further supported by measurements exploiting both discussed configurations [Figs. 3(b) and 3(d)], where a decrease and an increase of intensity, respectively, can be observed in the two cases. Here, the QD ensemble is used as an internal light source [40]. We recorded spectra for various cavity lengths with nanometric resolution. Each horizontal line represents a spectrum, whereas the intensity is color coded in a logarithmic scale. The anticrossing regime around 905 nm is well pronounced. The difference in spectral

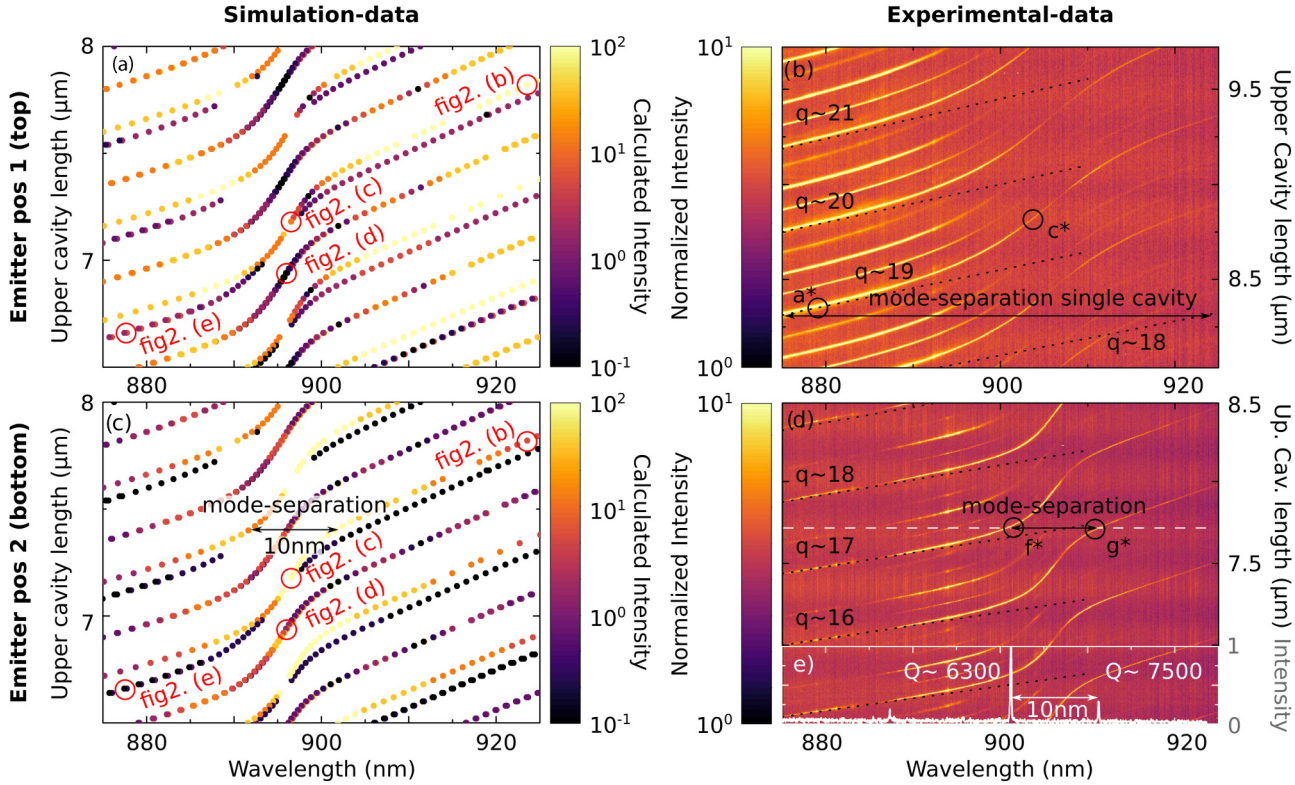

FIG. 3. Simulations [(a) and (c)] and experimental data [(b) and (d)] for a double cavity with 32 bottom, 9 middle, and 11 top DBR pairs. The cavity length of both the bottom and the GaAs part of the top cavity is set to the wavelength λ: For In(Ga)As quantum dots emitting around 900 nm, this results in a thickness of ≈260 nm. (a) and (b) show simulations for the expected intensity (product of calculated Purcell factor multiplied by the incoupling efficiency to the fiber) and corresponding experimental photoluminescence data for emitters implemented in the top cavity. (c) and (d) display simulation and experimental data, respectively, for emitters placed in the bottom cavity. For the measurement data [(b) and (d)], several spectra were acquired while increasing the length of the upper cavity (Up. Cav.) with nanometric resolution. Each horizontal line of the contour plot corresponds to a spectrum for a given cavity length. The respective intensities are color coded in a logarithmic scale for better visibility. Longitudinal and transversal modes can be clearly distinguished by their brightness and resemble the simulation data. Furthermore, the anticrossing regime is well pronounced. The black dashed lines are a guide to the eye for different cavity modes, q being the longitudinal mode number, in order to determine the effective cavity length. The black arrow in (b) indicates the separation of longitudinal modes for a single cavity (∼50 nm for the given cavity length). In contrast, the simulated (c) and experimentally achieved (d) mode separation is around 10 nm for the given geometry. The white dashed line in (d) indicates the position of the spectrum in subplot (e). Here, an exemplary spectrum is shown, indicating once again the mode separation as well as the Q factors of the longitudinal modes forming the supermode. Quality factors for the selected positions (a*, c*, f*, and g*) can be found in Table I.

position of simulation and experiment can be explained by a different thickness of the bottom cavity of a few nanometers between design and growth. Both longitudinal and transverse modes are clearly visible. Since in the experiment we cannot measure the mode-field profiles, it is not possible to distinguish longitudinal and transverse modes directly. Instead, we identify longitudinal modes by their higher brightness due to a better matching of their Gaussian beam profile to the collecting fiber and therefore a better light incoupling. Since the simulation of the mode profiles shows that in areas far detuned from the anticrossing, the modes manifest mainly in the upper cavity, we make the assumption that fitting the standard formula for determining cavity distances $L_{\text{eff}} = q\lambda/2$ is valid and derive the according cavity lengths in this way, attributing matching mode numbers to the longitudinal modes.

Focusing on the behavior of the longitudinal modes, we can demonstrate the creation of a coupled cavity system that has two modes with a spectral separation of a few nanometers [arrows in Figs. 3(c) and 3(d) as well as a cut-through shown in Fig. 3(e) displaying a single spectrum with a mode separation of 10 nm]. In a standard cavity with a similar geometry, the mode separation is ∼50 nm as depicted by the black arrow in Fig. 3(b). The mode separation of a double cavity structure strongly depends on the coupling strength of the resonators. A narrower separation can be achieved by increasing the number of mirror pairs of the middle DBR and therefore its reflectivity. This can be seen in Fig. 4, where the number of mirror pairs for the middle DBR is increased from 9 to 12 pairs and the mode separation is decreased to 5.5 nm. Careful design of the cavity geometry, especially its reflectivities, could allow achieving mode separations of around 3 nm, thus opening the path for various interesting experiments such as cavity-enhanced generation of entangled photons or twin photons where the modes can be matched to the biexciton or exciton transitions of an emitter. Furthermore, the separated modes can enhance both transitions with a high-quality factor.

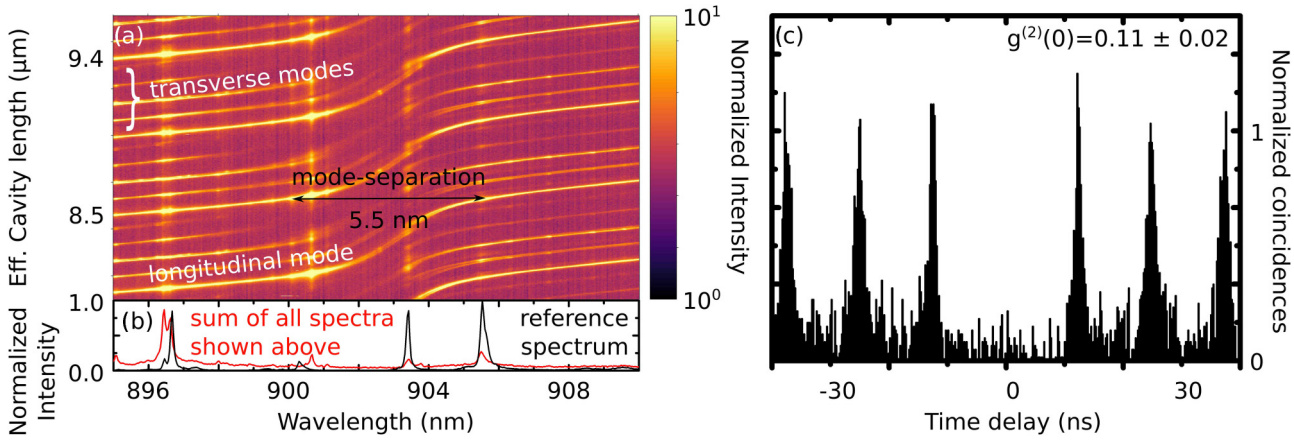

FIG. 4. Measurement data of an open cavity with 30 pairs of bottom DBRs, 12 pairs of middle DBRs, and 11 pairs of top DBRs. The bottom cavity is fabricated with a GaAs layer corresponding to 2.4λ, while the top GaAs layer is chosen to be 1λ for an emitter of $\lambda = 900$ nm in vacuum. The cavity is formed around a preselected InGaAs quantum dot placed in the top cavity. (a) Vertical scan of the fiber similar to the ones in Fig. 3. The bright vertical lines correspond to transitions of the embedded emitter. (b) For comparison, an artificial spectrum constructed out of the sum of the individual spectra in (a) is shown as a red line, and a reference spectrum of the quantum dot before placing it inside the cavity is shown in black. While the spectral features of the emitter transitions are still observable, the intensity distribution is modified due to a different light enhancement in the cavity structure. The brightness variation is consistent with the simulations in Fig. 3(a), where the Purcell enhancement is expected to be low in the anticrossing region and high outside. A small offset in wavelength arising from the usage of two different gratings has been accounted for. (c) Hanbury Brown and Twiss measurement performed for the quantum dot transition at 905.5 nm, revealing a second-order correlation value of $g^{(2)}(0) = 0.11 \pm 0.02$.

In order to observe two consecutive modes with a similar spectral separation in a standard cavity, it would be necessary to increase the distance between the mirrors significantly, therefore increasing the mode volume. This results in a considerable decrease in the achievable Purcell enhancement. To reach a mode separation similar to that depicted by the arrow in Fig. 3(d), the cavity length of a single cavity would be around 40 μm.

While the measurements up to this point have been conducted having off-resonant cavity feeding by the wetting layer and also by multiple QDs, in the following, one single QD is selected, and the cavity is formed around this QD. For this purpose, a state-of-the-art deterministic lithography machine [13] has been employed to preselect QDs emitting in the wavelength range of the measured anticrossing. Performing a similar scan of the cavity length as in Fig. 3, we collected the data shown in Fig. 4(a). The main difference from previously shown data can be found in the bright vertical lines, which correspond to transitions of the individual emitter. As demonstrated in our previous work [24], realizing markers via deterministic lithography and gold deposition enables us to find again the selected emitter even though the only source of information is the signal from the fiber itself. This becomes evident when comparing the spectrum of the emitter outside the cavity with the sum of the spectra in Fig. 4(a). This comparison is shown in Fig. 4(b): A clear correspondence in the observed resonances of the emitter between both measurement conditions can be seen. The intensity mismatch between the spectrum outside and the cumulative spectrum inside the cavity is due to the expected suppression of the signal in the anticrossing regime, when the QD is located in the top cavity (position 1 in Fig. 1). This behavior is also theoretically expected [see Fig. 3(a)].

To further prove the validity of the realized single-emitter-based cavity in quantum optical implementations, we performed a Hanbury Brown and Twiss measurement on one excitonic transition (905.5 nm). A value of the second-order correlation function of $g^2(0) = 0.11 \pm 0.02$ shows a low probability of creating multiphoton events.

V. CONCLUSION

In this study we designed, simulated, and implemented a tunable fiber-based open cavity showing two spectrally close resonances arising from two-mode hybridization. The spectral separation of the modes is of the order of only a few nanometers. This effect, which in monolithic cavities requires a precise control of the fabrication conditions, here is achieved by actively tuning the two modes into resonance. This is enabled by the combination of a double DBR monolithic structure with a high-reflectivity external fiber mirror. Interestingly, positioning the emitters in the bottom or top cavity modifies the expected Purcell enhancement, which experimentally manifests in a modification of the observed intensity for the two different configurations. Finally, thanks to the high level of control of the experimental conditions, a deterministically preselected QD is placed into the tunable cavity, showing the possibility of employing this novel double mode structure in quantum implementations.

ACKNOWLEDGMENTS

We thank C. Pauly for the fabrication of the fiber focused-ion-beam milling and L. Engel for the support in all clean-room steps. We greatly acknowledge the support of the Deutsche Forschungsgemeinschaft (DFG) via Project No. DFG MI500/31-1 and Program No. SPP1839, "Tailored Disorder."

[1] K. J. Vahala, Nature (London) **424**, 839 (2003).

[2] E. M. Purcell, H. C. Torrey, and R. V. Pound, Phys. Rev. **69**, 37 (1946).

[3] J. P. Reithmaier, G. Sek, A. Löffler, C. Hofmann, S. Kuhn, S. Reitzenstein, L. V. Keldysh, V. D. Kulakovskii, T. L. Reinecke, and A. Forchel, Nature (London) **432**, 197 (2004).

[4] E. Moreau, I. Robert, J. M. Gérard, I. Abram, L. Manin, and V. Thierry-Mieg, Appl. Phys. Lett. **79**, 2865 (2001).

[5] M. Pelton, C. Santori, J. Vucsković, B. Zhang, G. S. Solomon, J. Plant, and Y. Yamamoto, Phys. Rev. Lett. **89**, 233602 (2002).

[6] A. J. Bennett, D. C. Unitt, P. Atkinson, D. A. Ritchie, and A. J. Shields, Opt. Express **13**, 50 (2005).

[7] M. Schwab, H. Kurtze, T. Auer, T. Berstermann, M. Bayer, J. Wiersig, N. Baer, C. Gies, F. Jahnke, J. P. Reithmaier, A. Forchel, M. Benyoucef, and P. Michler, Phys. Rev. B **74**, 045323 (2006).

[8] X. Ding, Y. He, Z.-C. Duan, N. Gregersen, M.-C. Chen, S. Unsleber, S. Maier, C. Schneider, M. Kamp, S. Höfling, C.-Y. Lu, and J.-W. Pan, Phys. Rev. Lett. **116**, 020401 (2016).

[9] K. Srinivasan, P. E. Barclay, O. Painter, J. Chen, A. Y. Cho, and C. Gmachl, Appl. Phys. Lett. **83**, 1915 (2003).

[10] M. L. Gorodetsky, A. A. Savchenkov, and V. S. Ilchenko, Opt. Lett. **21**, 453 (1996).

[11] A. Dousse, L. Lanco, J. Suffczyński, E. Semenova, A. Miard, A. Lemaître, I. Sagnes, C. Roblin, J. Bloch, and P. Senellart, Phys. Rev. Lett. **101**, 267404 (2008).

[12] M. Gschrey, A. Thoma, P. Schnauber, M. Seifried, R. Schmidt, B. Wohlfeil, L. Krüger, J.-H. Schulze, T. Heindel, S. Burger, F. Schmidt, A. Strittmatter, S. Rodt, and S. Reitzenstein, Nat. Commun. **6**, 7662 (2015).

[13] M. Sartison, S. L. Portalupi, T. Gissibl, M. Jetter, H. Giessen, and P. Michler, Sci. Rep. **7**, 39916 (2017).

[14] L. Sapienza, M. Davanço, A. Badolato, and K. Srinivasan, Nat. Commun. **6**, 7833 (2015).

[15] R. Albrecht, A. Bommer, C. Deutsch, J. Reichel, and C. Becher, Phys. Rev. Lett. **110**, 243602 (2013).

[16] H. Kaupp, T. Hümmer, M. Mader, B. Schlederer, J. Benedikter, P. Haeusser, H.-C. Chang, H. Fedder, T. W. Hänsch, and D. Hunger, Phys. Rev. Appl. **6**, 054010 (2016).

[17] B. Besga, C. Vaneph, J. Reichel, J. Estève, A. Reinhard, J. Miguel-Sánchez, A. Imamoğlu, and T. Volz, Phys. Rev. Appl. **3**, 014008 (2015).

[18] L. Greuter, S. Starosielec, A. V. Kuhlmann, and R. J. Warburton, Phys. Rev. B **92**, 045302 (2015).

[19] D. Najer, M. Renggli, D. Riedel, S. Starosielec, and R. J. Warburton, Appl. Phys. Lett. **110**, 011101 (2017).

[20] D. Najer, I. Söllner, P. Sekatski, V. Dolique, M. C. Löbl, D. Riedel, R. Schott, S. Starosielec, S. R. Valentin, A. D. Wieck, N. Sangouard, A. Ludwig, and R. J. Warburton, Nature (London) **575**, 622 (2019).

[21] F. Li, Y. Li, Y. Cai, P. Li, H. Tang, and Y. Zhang, Adv. Quantum Technol. **2**, 1900060 (2019).

[22] A. Muller, E. B. Flagg, M. Metcalfe, J. Lawall, and G. S. Solomon, Appl. Phys. Lett. **95**, 173101 (2009).

[23] J. Miguel-Sánchez, A. Reinhard, E. Togan, T. Volz, A. Imamoglu, B. Besga, J. Reichel, and J. Estève, New J. Phys. **15**, 045002 (2013).

[24] T. Herzog, M. Sartison, S. Kolatschek, S. Hepp, A. Bommer, C. Pauly, F. Mücklich, C. Becher, M. Jetter, S. L. Portalupi, and P. Michler, Quantum Sci. Technol. **3**, 034009 (2018).

[25] A. Dousse, J. Suffczyński, A. Beveratos, O. Krebs, A. Lemaître, I. Sagnes, J. Bloch, P. Voisin, and P. Senellart, Nature (London) **466**, 217 (2010).

[26] M. Benyoucef, J.-B. Shim, J. Wiersig, and O. G. Schmidt, Opt. Lett. **36**, 1317 (2011).

[27] S. Seyfferle, F. Hargart, M. Jetter, E. Hu, and P. Michler, Phys. Rev. B **97**, 035302 (2018).

[28] K. A. Atlasov, K. F. Karlsson, A. Rudra, B. Dwir, and E. Kapon, Opt. Express **16**, 16255 (2008).

[29] P. Michler, M. Hilpert, and G. Reiner, Appl. Phys. Lett. **70**, 2073 (1997).

[30] A. Armitage, M. S. Skolnick, V. N. Astratov, D. M. Whittaker, G. Panzarini, L. C. Andreani, T. A. Fisher, J. S. Roberts, A. V. Kavokin, M. A. Kaliteevski, and M. R. Vladimirova, Phys. Rev. B **57**, 14877 (1998).

[31] D. Marcuse, IEEE J. Quantum Electron. **21**, 1819 (1985).

[32] G. Panzarini, L. C. Andreani, A. Armitage, D. Baxter, M. S. Skolnick, V. N. Astratov, J. S. Roberts, A. V. Kavokin, M. R. Vladimirova, and M. A. Kaliteevski, Phys. Rev. B **59**, 5082 (1999).

[33] R. P. Stanley, R. Houdré, U. Oesterle, M. Ilegems, and C. Weisbuch, Appl. Phys. Lett. **65**, 2093 (1994).

[34] A. A. P. Trichet, P. R. Dolan, D. M. Coles, G. M. Hughes, and J. M. Smith, Opt. Express **23**, 17205 (2015).

[35] COMSOL, COMSOL MULTIPHYSICS v. 5.4, Stockholm, 2018, https://www.comsol.com.

[36] S. Gehrsitz, F. K. Reinhart, C. Gourgon, N. Herres, A. Vonlanthen, and H. Sigg, J. Appl. Phys. (Melville, NY) **87**, 7825 (2000).

[37] T. J. Bright, J. I. Watjen, Z. M. Zhang, C. Muratore, A. A. Voevodin, D. I. Koukis, D. B. Tanner, and D. J. Arenas, J. Appl. Phys. (Melville, NY) **114**, 083515 (2013).

[38] I. H. Malitson, J. Opt. Soc. Am. **55**, 1205 (1965).

[39] C. Sauvan, J. P. Hugonin, I. S. Maksymov, and P. Lalanne, Phys. Rev. Lett. **110**, 237401 (2013).

[40] J. M. Gerard and B. Gayral, J. Lightwave Technol. **17**, 2089 (1999).